

# Cyclotron trap

D. Gotta<sup>1\*</sup> and L.M. Simons<sup>2</sup>

<sup>1</sup> Institut für Kernphysik, Forschungszentrum Jülich, D-52425 Jülich, Germany

<sup>2</sup> Paul Scherrer Institut, CH-5232 Villigen, Switzerland

\* d.gotta@fz-juelich.de

March 11, 2021



*Review of Particle Physics at PSI*

doi:[10.21468/SciPostPhysProc.2](https://doi.org/10.21468/SciPostPhysProc.2)

## Abstract

The cyclotron trap was developed at SIN/PSI to increase the stopping density of negatively charged particle beams for the formation of exotic atoms in low pressure gases. A weak focusing magnetic field, produced by superconducting solenoids, is used. Particles are injected radially through the fringe field to a moderator, which decelerates them into orbits bound by the field. Further deceleration by moderators and/or low-pressure gases leads the particles to the centre of the device, where they can be stopped or eventually extracted. Experiments became feasible with this technique, such as those dealing with pionic hydrogen/deuterium at SIN/PSI. Muonic hydrogen laser experiments also became possible with the extraction of muons from the cyclotron trap. The formation of antiprotonic hydrogen in low pressure targets led to successful experiments at LEAR/CERN.

## 13.1 Introduction

The advent of meson factories in the 70's and of the antiproton factory LEAR in the 80's, resulted in a revival of interest in the physics of exotic atoms. Before then, the main focus of research was the investigation of nuclear charge parameters with muonic atoms, and the determination of the strong interaction shift and broadening in hadronic atoms [1]. Experiments had been almost exclusively performed in medium- to high- $Z$  solid or high-pressure targets. Exotic atoms were produced by decelerating the beam particles with a linear array of low- $Z$  moderators, such as  $Be$ ,  $CH_2$ , or  $C$  to minimize straggling.

This technique was sufficient for the purposes at that time, but was not adequate for experiments of more fundamental interest. Such experiments have in common the need of low-pressure gas targets. As an example, neutral exotic hydrogen/deuterium atoms can penetrate deeply into the field of neighbouring atoms. At higher pressures they are destroyed by the Stark effect before they can emit the X-rays one wants to measure [2].

A second example is given by exotic atoms of higher  $Z$  gases. Here, a completely ionized electron shell can keep the exotic atom free from interactions with neighbouring atoms, thus approaching the state of an ideal exotic atom. The X-rays in question, with energies in the keV region, suffer self-absorption in high  $Z$  gases. In addition, thin windows must be used. Both reasons argue against high-pressure gas targets.

Experiments planned at LEAR/CERN to measure X-rays from antiprotonic hydrogen and deuterium, motivated a new technique to stop particles at the lowest pressures. The cyclotron trap (CTI), developed and built by a group from the University of Karlsruhe

42 working at SIN and at LEAR, met this requirement. CTI was used both at LEAR with  
 43 antiprotons, and at SIN/PSI with pions and muons. A second instrument (CTII) was  
 44 developed later, specially tailored to the pion and muon beams at PSI.

### 45 13.2 The basic principle

46 In the following, cylindrical coordinates are used, with  $r$ ,  $\theta$ , and  $z$  for radius, azimuthal  
 47 angle, and axial direction, respectively.

48 The working principle of the cyclotron trap is to wind up the range path of particles  
 49 inside a rotationally symmetric weak-focusing magnetic field  $B$  characterized by  $0 \leq n \leq 1$ ,  
 50 where  $n$  is the field index given by

$$n = -(\delta B / \delta r) \cdot (r / B) . \quad (13.1)$$

51 Particles with momenta  $p_{beam}$  are injected radially through the fringe field to a radius  
 52  $r_{in}$  in a direction opposite to that for ejection from a cyclotron accelerator. At this radius  
 53 they are decelerated by a moderator to momenta  $p_\theta$

$$p_\theta = -\frac{e}{c} B_z \cdot r_{in} , \quad (13.2)$$

54 which ideally leads to circular orbits at a given field  $B_z$ . A deviation from this ideal picture  
 55 is caused by the injection method itself. Betatron oscillations are deliberately excited at  
 56 injection for radii with  $0.5 \leq n \leq 0.8$  to prevent the particles from hitting the moderator  
 57 in one of the subsequent revolutions. More important is the radial spread  $\Delta r_p$  caused by  
 58 the momentum spread  $\Delta p$  from deceleration in the injection moderator. This depends  
 59 strongly on the injection scheme chosen for the different particle beams and is given by

$$\Delta r_p = r \cdot \frac{\Delta p}{p} \cdot \frac{1}{1 - n} . \quad (13.3)$$

60 This leads to spreads of a few millimeters for antiproton beams at LEAR, and to a few  
 61 centimeters for pion injection at SIN/PSI as the worst case. Assuming a smooth energy  
 62 loss beyond this point, the particles can then be guided by the weak focusing cyclotron  
 63 field and be led to the centre of the device.

64 A first comparison with a linear arrangement for stopping particles with range length  $R$   
 65 is given here. For a linear arrangement, the stopping process leads to a longitudinal range  
 66 straggling,  $\delta R$ , and Coulomb scattering leads to a lateral widening of the order of  $2 \cdot \delta R$ .  
 67 The stopping volume then is of the order of  $4 \cdot (\delta R)^3$  [3]. With the cyclotron trap, the  
 68 range is wound up into a spiral with its end at the centre of the cyclotron trap, yielding,  
 69 in first approximation, a radial spread of  $\Delta r_{stop} = r_{in} \cdot \delta R / R$ . The uncertainty in range  
 70 leads only to an azimuthal uncertainty and multiple scattering leads to a broadening in the  
 71  $z$  direction. If the deceleration is slow enough, the orbits would adiabatically follow the  
 72 shrinking radius corresponding to the decreasing momentum  $p$ . The stopping distribution  
 73 in the cyclotron trap scales with the value for the injection radius, so that a stopping  
 74 volume is:

$$V_{stop}^{cyc} \propto \left( r_{in} \cdot \frac{\delta R}{R} \right)^3 . \quad (13.4)$$

75 A gain of the order of  $(\frac{R}{r_{in}})^3$ , compared with a linear degrader arrangement, can, in  
 76 principle, be reached. In practice, the gain factor is smaller. This is caused mainly for  
 77 pions by the short lifetime requiring the use of additional moderators. For pion and muon  
 78 beams, losses occur during the injection through the fringe field because of the quality of

79 the beam. In addition, range straggling in the moderator and deliberate detuning in the  
 80 beginning of the deceleration process must be taken into account for all types of particles.  
 81 These factors result in an additional increase of the stopping distribution.

82 For antiprotons, a gain factor of  $10^4$  was measured. For pions and muons, gain factors  
 83 of the order of 10 to 30 proved to be realistic.

### 84 13.3 The principle in more detail

85 An instructive way to visualize the principle of the cyclotron trap is given by the quasipo-  
 86 tential picture [4, 5]. The quasipotential  $U(r, z)$  is given by

$$U(r, z) = \frac{1}{2m} \cdot \left( \frac{P}{r} - \frac{e}{cr} \cdot \int_0^r B_z(r', z) r' dr' \right)^2 \quad (13.5)$$

87 with  $P$  being the so-called generalized angular momentum

$$P = r p_\theta + \frac{e}{c} \int_0^r B_z(r', z) r' dr' = \text{const} \quad (13.6)$$

88 Values for the quasipotential are depicted in Figure 13.1 and in Figure 13.2 for the  
 89 field of CTI. Bound orbits require minima of the quasipotential curves both in radial and  
 90 axial direction. This leads to the requirement  $0 < n < 1$ . For the minima in  $U(r, z = 0)$   
 91 the radius of an orbiting particle is given by equation (13.2).

92 As seen from Figure 13.1, values of  $P$  higher than about 6 MeV/c-m cannot lead to  
 93 bound orbits as minima develop only for smaller values. The injection, e.g. of antiprotons  
 94 with a momentum of 200 MeV/c, requires a momentum loss of 70 MeV/c in a moderator  
 95 of suitable thickness placed at a radius of about 140 mm. In this way they are captured  
 96 in a shallow potential well with  $P$  slightly lower than 6 MeV/c-m. Without any further  
 97 energy loss, the particles would be stopped in one of the next orbits by this moderator. If  
 98 there is an additional energy loss, they eventually follow the developing potential minima.  
 99 If the energy loss is sufficiently small, the particles oscillate around the newly established  
 100 equilibrium radii and will be guided adiabatically to the centre of the trap. If the energy  
 101 loss is too large, the centre of the device will not be included in the orbit of the particles.  
 102 A negative generalized momentum would develop and the particles would even be expelled  
 103 from the centre [5].

104 In the axial direction the focusing is very strong in the beginning of the deceleration  
 105 process, and decreases when the particles orbit to the centre of the cyclotron trap. They  
 106 will be stopped at short axial distances from the centre because of their low energy. In  
 107 addition the magnetic mirror effect will contain them axially. Applying an axial electric  
 108 field provides the opportunity to extract them to form a particle beam. This approach  
 109 was used to provide a low-energy muon beam for an experiment to determine the proton  
 110 radius mentioned in Section 13.6.2.

### 111 13.4 Phase space considerations

112 The phase space development in the case of energy loss is described by the extended  
 113 Liouville theorem [6]. For the deceleration of particles in matter the dissipative force  
 114 given by the energy loss (Bethe-Bloch formula) can be approximated as a function of the  
 115 momentum  $p$  by

$$Q \propto p^{\alpha(p)} . \quad (13.7)$$

116 The value of  $\alpha$  varies between  $-1.4$  and  $-1.7$  for materials with low ionization potentials.  
 117 Assuming  $\alpha$  is piecewise constant, and partitioning the deceleration path into constant

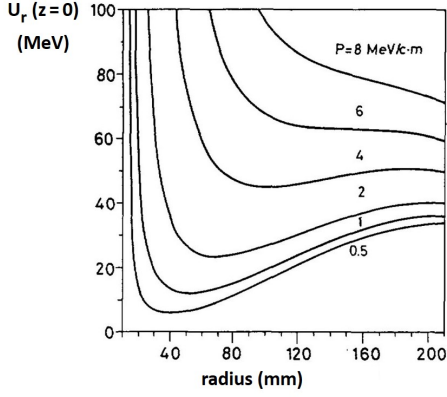


Figure 13.1: Radial distribution of the quasipotential in the median plane for different positive values of the generalized momentum  $P$ .

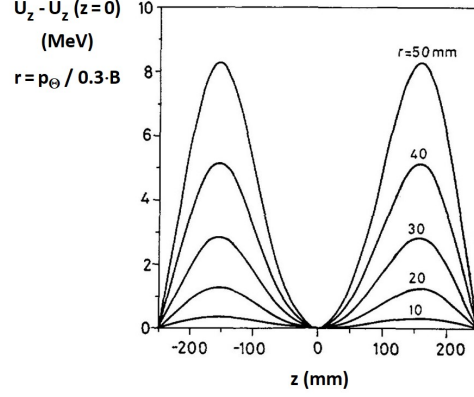


Figure 13.2: The difference of the axial distribution of the quasipotential to its value at  $z = 0$  is shown for different values of the equilibrium radii  $r_0$ .

118 time intervals, the ratio of the momentum spread at the beginning (i) and the end (f) of  
 119 an interval is given by

$$\frac{\Delta p_f}{\Delta p_i} = \left( \frac{p_f}{p_i} \right)^\alpha. \quad (13.8)$$

120 This relation does not hold if the emittance changes during deceleration, as is the case for  
 121 the deceleration by an electric field. Energy loss, however, applies equally in any spatial  
 122 direction resulting in a constant emittance. Going from linear to circular motion, we arrive  
 123 at an expression that is central for understanding the working principle of the cyclotron  
 124 trap

$$\frac{\Delta p_f}{\Delta p_i} = \left( \frac{p_f}{p_i} \right)^\alpha \cdot \frac{\omega_i}{\omega_f} \quad (13.9)$$

125 with  $\omega$ , the circular frequency of motion, being proportional to the magnetic field strength.  
 126 The increase of  $\Delta p$ , caused by the momentum decrease, is partially counteracted by the  
 127 increase of the cyclotron frequency at smaller radii. The interesting quantity for the  
 128 formation of exotic atoms, however, is the radial spread  $\Delta r_p$ . It is connected to the  
 129 momentum spread via equation (13.3). For the orbits with small radii and  $n$  approaching  
 130 a value of 0, a decrease of  $\Delta r_p$  can be expected.

131 Extensive calculations of the dynamics of the injected and decelerated particles with  
 132 real beam parameters and the geometry of the finally-built cyclotron traps confirmed these  
 133 expectations. The radial extension of the stopping distribution corresponds to the radial  
 134 spread of the beam at the beginning of the deceleration process. The axial extension of  
 135 the stopping distribution, however, is almost a factor of 2 bigger than the axial extension  
 136 at the beginning.

### 137 13.5 Technical realisation

138 The weak focusing field is produced by two superconducting ring coils. Because of the  
 139 high field strength, the dimensions of the device can be kept small. The field direction  
 140 is horizontal so that the particle orbits are in the vertical plane. Access to the stopping  
 141 region is provided by a borehole in the cryostat housing of the coils. We describe here the  
 142 set-up of CT II shown in Figure 13.3 and Figure 13.4.

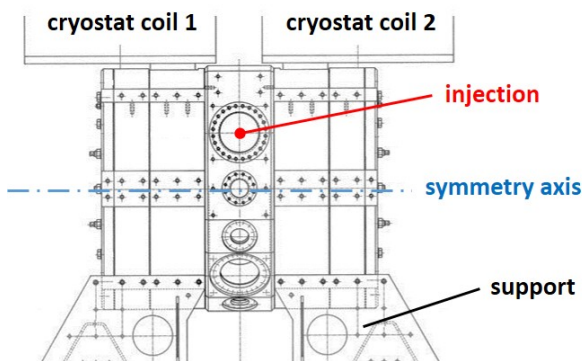


Figure 13.3: The set-up of CT II. The magnetic field is horizontal with the injection point in the vertical symmetry plane, about 200 mm from the symmetry axis. The supporting table and the two separated cryostats are indicated.

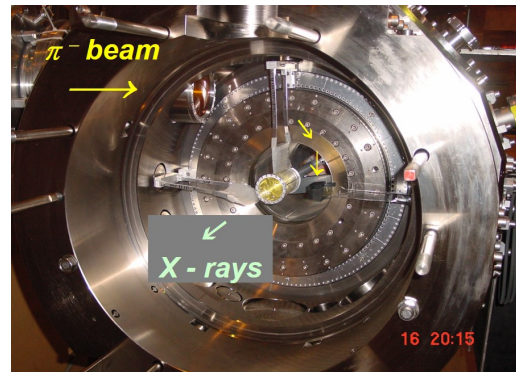


Figure 13.4: The interior part of CT II with one of the two halves removed. The beam enters from the left and is guided to a gas target on the symmetry axis with the help of additional moderators.

143 The two superconducting coils are located in separated cryostats. They are surrounded  
 144 by a soft iron return yoke that also serves as magnetic shielding to reduce the fringe field.  
 145 Additional soft iron pieces are mounted at the inner cryostat walls to optimize the field.  
 146 Iron rings are mounted to balance magnetic forces. Beams are injected through a hole  
 147 in the shielding as shown in Figure 13.4. The two halves can be separated to access the  
 148 interior, thus providing a high versatility.

## 149 13.6 Particle physics experiments

150 As most of the experiments performed with the two cyclotron traps were discussed in a  
 151 review paper by D. Gotta [7] including extensive references, the following discussion can  
 152 be brief.

### 153 13.6.1 Antiprotonic atoms

154 The possibility of experiments with antiprotonic atoms at LEAR/CERN motivated the  
 155 construction of the cyclotron trap CTI. The 105 MeV/c antiproton beams were ideal for  
 156 the deceleration with the cyclotron trap. Of the incoming beam, 86% can be stopped in  
 157 a 30 mbar hydrogen gas target with a diameter of 20 mm (FWHM). This resulted in an  
 158 increase of stopping densities of more than 4 orders of magnitude, and led to successful  
 159 measurements of the ground state shift and width in antiprotonic hydrogen isotopes. A  
 160 measurement of these quantities for the  $2p$ -state in these atoms with a crystal spectrometer  
 161 was also made [8].

### 162 13.6.2 Muonic and pionic atoms

163 The muon and pion beams at SIN/PSI presented considerable difficulties for the use of the  
 164 cyclotron trap. The emittance of the beams and the lifetimes of the particles, deviated  
 165 from the ideal situation encountered with antiprotons. Nonetheless, experiments with  
 166 the first cyclotron trap (CTI) proved to be successful. In a first experiment, the pion  
 167 mass was determined from pionic atoms formed in nitrogen gas with an almost depleted  
 168 electron shell [9]. Earlier experiments suffered from the lack of knowledge of the state of  
 169 the electron shell, as a solid Mg target was used. The determination of the pion mass was

170 later improved by using CT II, allowing for energy calibration with muonic oxygen [10]  
171 (Section 10 [11]). Coulomb explosion was directly observed for the first time; this occurs  
172 in the formation of exotic atoms from molecules such as  $N_2$  [12]. A first round of crystal  
173 spectrometer measurements of X-rays in pionic hydrogen isotopes was also performed. The  
174 work with muonic atoms led to the observation of the two-photon transition in muonic  
175 boron [13].

176 The second cyclotron trap (CT II) was developed to adapt its acceptance to the emit-  
177 tance of the pion and muon beams at PSI. For pions, about 1% of the initial beam could  
178 be stopped in a hydrogen target at STP. For muon beams, this number is about one order  
179 of magnitude higher. This led to a successful series of measurements in muonic hydrogen  
180 and in both pionic hydrogen and deuterium, reducing typical measuring times to a month  
181 (Section 14 [14]). The line shape of the muonic hydrogen  $K\beta$  transition was determined  
182 with high precision as a prerequisite for later experiments in pionic hydrogen [15]. A  
183 method was developed to extract muons from the centre of the trap to form a low-energy  
184 muon beam. This opened a path for important experiments to determine the proton radius  
185 via the Lamb shift in muonic hydrogen [16] (Section 21 [17]).

## 186 13.7 Atomic physics experiments

### 187 13.7.1 Ionized exotic atoms

188 It became clear at an early stage that the possibility of forming exotic atoms in low  
189 pressure gases can lead to a complete ionization of the electron shell [18]. After formation,  
190 the electromagnetic cascade depletes the electron shell up to  $Z = 36$  for antiprotons, and  
191 up to  $Z = 18$  for muons or pions. As the natural linewidth of the corresponding transitions  
192 is negligibly small, these X-rays can be used for calibration of some atomic and particle  
193 physics experiments [10, 19]. The atomic physics aspect of these experiments proved to be  
194 interesting by itself [20, 21].

### 195 13.7.2 ECR-source: a by-product

196 The crystal spectrometer experiment in pionic hydrogen and deuterium required a precise  
197 knowledge of the response function of the device. To achieve this, the of geometry CTII  
198 was changed to that of an ECR source providing a high-intensity X-ray source. Here the  
199 distance of the solenoids had to be changed and a hexapole was inserted on the axis of  
200 CTII [22]. Then, the crystal spectrometer could be calibrated in a set-up equivalent to  
201 the pionic and muonic experiments [23].

## 202 References

- 203 [1] J. Hüfner, F. Scheck and C. S. Wu, *Muon physics I*, Academic Press, New York  
204 (1977).
- 205 [2] E. Borie and M. Leon, *X-ray yields in protonium and mesic hydrogen*, Phys. Rev. A  
206 **21**, 1460 (1980).
- 207 [3] L. M. Simons *et al.*, *Exotic atoms and their electron shell*, Nucl. Instr. and Meth. B  
208 **87**, 293 (1994).
- 209 [4] A. A. Kolomensky and A. N. Lebedev, *Theory of Cyclic Accelerators*, North-Holland  
210 Publishing Company, Amsterdam (1966).

- 211 [5] L. M. Simons, *Recent results on antiprotonic atoms using a cyclotron trap at LEAR*,  
212 *Physica Scripta* **T22** (1988).
- 213 [6] A. J. Lichtenberg, *Phase space dynamics of particles*, J. Wileys, New York (1969).
- 214 [7] D. Gotta, *Precision spectroscopy of light exotic atoms*, *Progr. Part. Nucl. Phys.* **52**,  
215 133 (2004).
- 216 [8] D. Gotta *et al.*, *Balmer  $\alpha$  transitions in antiprotonic hydrogen and deuterium.*, *Nucl.*  
217 *Phys. A* **660**, 283 (1999).
- 218 [9] S. Lenz *et al.*, *A new determination of the mass of the charged pion*, *Phys. Lett. B*  
219 **416**, 50 (1998).
- 220 [10] M. Trassinelli *et al.*, *Measurement of the charged pion mass using X-ray spectroscopy*  
221 *of exotic atoms*, *Phys. Lett. B* **759**, 583 (2016).
- 222 [11] M. Daum and D. Gotta, *The mass of the  $\pi^-$* , *SciPost Phys. Proc.* **2**, ppp (2021),  
223 doi:[10.21468/SciPostPhysProc.2.XXX](https://doi.org/10.21468/SciPostPhysProc.2.XXX).
- 224 [12] T. Siems *et al.*, *First direct observation of Coulomb explosion during the formation*  
225 *of exotic atoms*, *Phys. Rev. Lett.* **84**, 4573 (2000).
- 226 [13] K. Kirch *et al.*, *Metastability of the muonic boron 2s state*, *Phys. Rev. Lett* **78**, 4363  
227 (1997).
- 228 [14] D. Gotta and L. M. Simons, *Pionic hydrogen and deuterium*, *SciPost Phys. Proc.* **2**,  
229 ppp (2021), doi:[10.21468/SciPostPhysProc.2.XXX](https://doi.org/10.21468/SciPostPhysProc.2.XXX).
- 230 [15] D. S. Covita *et al.*, *Line shape analysis of the  $K\beta$  transition in muonic hydrogen*,  
231 *Eur. Phys. J. D* **72**, 72 (2018).
- 232 [16] A. Antognini *et al.*, *Proton structure from the measurement of the 2s – 2p*  
233 *transition frequencies of muonic hydrogen*, *Science* **339(6118)**, 417 (2013),  
234 doi:[10.1126/science.1230016](https://doi.org/10.1126/science.1230016).
- 235 [17] A. Antognini, F. Kottmann and R. Pohl, *CREMA*, *SciPost Phys. Proc.* **2**, ppp (2021),  
236 doi:[10.21468/SciPostPhysProc.2.XXX](https://doi.org/10.21468/SciPostPhysProc.2.XXX).
- 237 [18] R. Bacher *et al.*, *Muonic atoms with vacant electron shells*, *Phys. Rev. Lett.* **54**, 2087  
238 (1985).
- 239 [19] D. F. Anagnostopoulos *et al.*, *Low-energy X-ray standards from hydrogenlike pionic*  
240 *atoms*, *Phys. Rev. Lett.* **91**, 240801 (2003).
- 241 [20] K. Kirch *et al.*, *Muonic cascades in isolated low-Z atoms and molecules*, *Phys. Rev.*  
242 *A* **59**, 3375 (1999).
- 243 [21] D. Gotta *et al.*, *X-ray transitions from antiprotonic noble gases*, *Eur. Phys. J. D* **47**,  
244 11 (2008).
- 245 [22] S. Biri *et al.*, *Electron cyclotron resonance ion trap: A hybrid magnetic system with*  
246 *very high mirror ratio for highly charged ion production and trapping.*, *Review of*  
247 *Scientific Instruments* **71**, 1116 (2000).
- 248 [23] D. F. Anagnostopoulos *et al.*, *On the characterisation of a Bragg spectrometer with*  
249 *X-rays from an ECR source.*, *Nucl. Instr. and Meth. A* **545**, 217 (2005).